THE JOURNAL OF PHYSICAL CHEMISTRY C
A JOURNAL OF THE AMERICAN CHEMICAL SOCIETY

pubs.acs.org/JPCC

Article

Diels–Alder Reaction in a Molecular Junction

Leopoldo Mejía,[§] Diego Garay-Ruiz,[§] and Ignacio Franco*

Cite This: *J. Phys. Chem. C* 2021, 125, 14599–14606

Read Online

ACCESS | Metrics & More | Article Recommendations | Supporting Information

ABSTRACT: We computationally investigate the utility of molecular junctions to probe chemical reactivity at the single-molecule limit. To do so, we employ molecular dynamics (MD) coupled to quantum transport simulations to investigate the classic Diels–Alder reaction but in the context of nanoscale junctions where the reactants are nanoconfined and the reactive pair is mechanically brought to proximity. To capture reactive events, the MD employs the density functional tight binding method to account for interatomic interactions. To understand the thermodynamic driving forces behind the reaction in this novel chemical environment, we reconstruct the potential of mean force along the reaction coordinate and decompose it into energetic and entropic contributions. The analysis demonstrates that the process is entropically penalized, which makes the reaction barrier sensitive to changes in the temperature and reactant rigidity. The simulations further show that in nanojunctions the degree of reactivity can be mechanically manipulated simply by controlling the proximity of the electrodes. Surprisingly, for optimal electrode separations, the entropic and energetic cost in the nanoconfined reaction coincides with that observed in bulk, establishing a clear connection between measurements performed in these two vastly different reactive environments. Finally, we show how conductance measurements can be used to experimentally monitor the process at the single-entity limit.

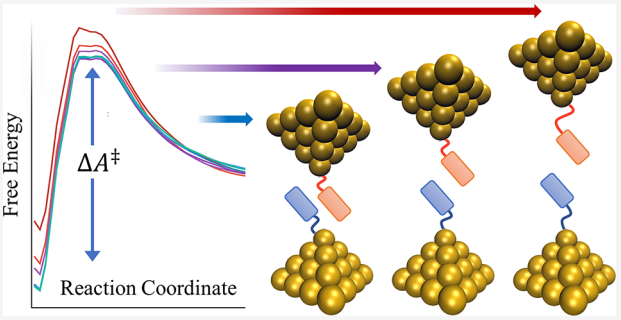

INTRODUCTION

Single-molecule junctions (SMJs) are formed when one molecule bridges the gap between two metallic electrodes. This setup serves as a platform to investigate fundamental physics and chemistry at the single-molecule limit. Specifically, in this chemical environment the molecular properties are probed by applying external stimuli, such as bias voltages or mechanical forces. This has led to detailed investigations of charge,[1−4] heat,[5−7] and spin[8,9] transport in molecules, quantum interference effects,[10−12] and the development of multidimensional single-molecule spectroscopies.[13−15] SMJs have also been used to construct molecular devices including switches,[16,17] transistors,[18−21] and diodes.[22,23]

An emergent frontier in this field is to investigate chemical reactivity. Examples include molecular switches based on photoinduced ring opening/closing reactions,[24] the study of nucleophilic addition,[25] mechanically activated redox events,[26] electrostatic catalysis of cycloadditions,[27] photothermal reactions,[28] and mechanically activated isomerizations of cyclopropane rings.[13]

The advantage of the SMJ setup is that it enables investigating chemical events at the single reactive entity limit. Nevertheless, these reactions occur in a nanoconfined environment where reactants and products are tethered to macroscopic electrodes. It is thus natural to ask: (i) What is the relation, if any, between chemical reactivity in bulk and in a nanojunction setting? (ii) How does the nanoconfinement influence its thermodynamic cost? (iii) To what extent can the mechanical manipulation be employed to control reactive outcomes?

Here we computationally approach these questions by investigating the Diels–Alder (DA) reaction in a Au–molecule–Au junction setting where the reactants are nanoconfined and the reactive pair is mechanically brought to proximity (as schematically shown in Figure 1a). The DA reaction, in which a diene and a dienophile form a cyclohexene derivative through a cyclic transition state, have been used extensively in chemical synthesis due to their robustness to experimental conditions, low activation energy barriers, and the variety of chemical motifs and substituents that can be employed.[29−33] It is therefore both an exemplifying and practical choice for studies of reactivity at the single-entity limit.

As discussed below, the activation energy and stability of the products of the DA reaction can be tuned by mechanically changing the separation distance between the electrodes, *L*. Rather surprisingly, when the junction reaches a range of

Received: March 2, 2021
Revised: June 14, 2021
Published: June 29, 2021

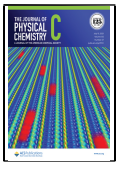

https://doi.org/10.1021/acs.jpcc.1c01901
J. Phys. Chem. C 2021, 125, 14599–14606

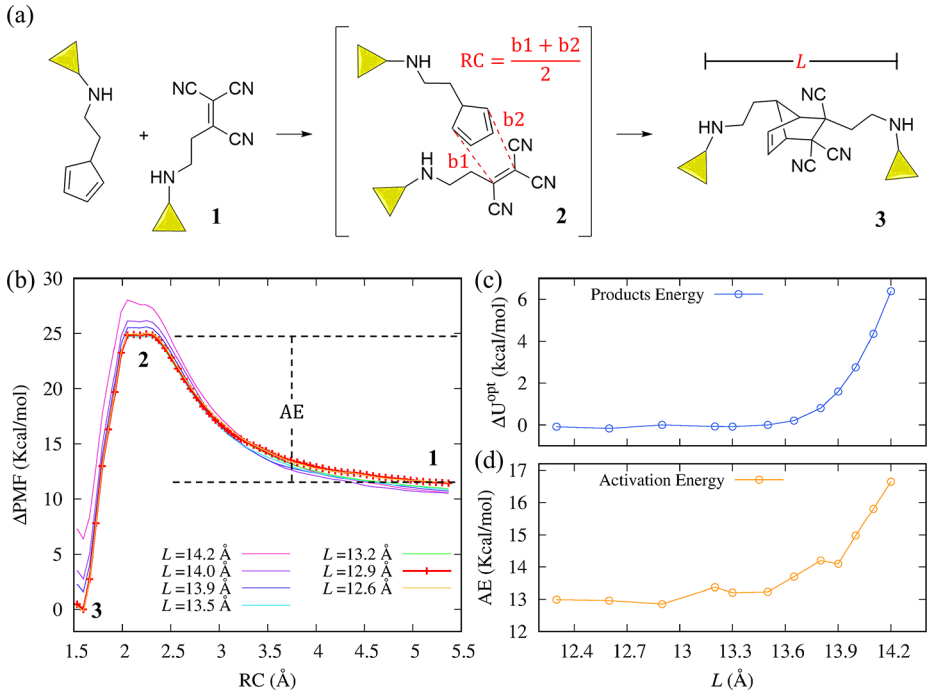

Figure 1. Relative potential of mean force (ΔPMF) and thermodynamic properties of the Diels–Alder (DA) reaction in a junction. (a) Representation of the DA reaction between substituted ethylene and cyclopentadiene to form a molecular junction. The yellow triangles represent gold electrodes; b_1 and b_2 indicates the position of the bonds being formed in the reaction, whose length is used to define the reaction coordinate (RC). (b) ΔPMF for the DA reaction considering different separation lengths between electrodes, *L*. The crossed red line highlights the ΔPMF with the lowest activation energy. **1**, **2**, and **3** signal the position of the corresponding stages of the reaction on the PMF profile. (c) Relative energy of the DA product, corresponding to the optimized geometry of the system in the products region, as a function of *L*. (d) Activation energy of the DA reaction as a function of *L*. Note that the thermodynamics of the DA reaction is highly sensitive to variations of *L*.

optimal distances between the electrodes, the process recovers the same thermodynamic features of the bulk reaction where reactants are not attached to electrodes.

METHODS

Diels–Alder Reaction. The challenge of simulating the dynamics of a chemical reaction is that bond rupture and forming events need to be described with quantum mechanics. However, the computational cost of a full quantum dynamics simulation is prohibitive for large systems and long times, such as the ones considered here. By contrast, classical molecular dynamics allows for computationally accessible simulations. However, most classical force fields do not permit bond rupture and forming processes. One alternative is to use reactive force fields,[34,35] but this kind of force field is limited to describe very specific reactions and atom types.

To overcome this problem, we performed classical molecular dynamics (MD) simulations using the density functional tight-binding method with self-consistent charges (SCC-DFTB) to compute the interatomic forces. The SCC-DFTB Hamiltonian allows the description of quantum events at an accuracy similar to that of density functional theory (DFT) methods but at a lower computational cost due to its semiempirical nature. The atomistic simulation environment (ASE)[36] was used as the MD driver, with DFTB+[37] as the force calculator using the *auorg* Slater–Koster parameters.[38] The temperature (300 K unless explicitly mentioned) was fixed by applying a Langevin thermostat with a damping factor of 50 fs, and the equations of motion were propagated using an integration time step of 1.0 fs. To incorporate the effects of the electrodes in the molecular dynamics, we attached the reactants to a five-atom square-base Au pyramid using amino anchor groups, as schematically represented in Figure 1a. We choose deprotonated NH amines rather than the NH_2 linkers that coordinate to the Au through their electron lone pair because the *auorg* parameters are designed to describe covalent N–Au interactions. Experimentally, this kind of anchor group has been shown to lead to enhanced transport.[39] The electrode–electrode distance, *L*, was kept fixed during the simulations by attaching the tip-atom of each electrode to stiff virtual springs. All other Au atoms were allowed to move. The parameter *L* was then systematically changed to evaluate the effect of varying the distance between electrodes due to the mechanical manipulation of the junction.

The simulation strategy assumes that any applied voltage in the junction setting is low enough such that it does not influence the molecular dynamics of the reactive pair. The possible use of electric fields to catalyze the DA reaction has been investigated previously.[27]

At the single-molecule limit, chemical reactions are rare events. A typical DA reaction with an activation free energy (AE) of 12.66 kcal/mol would take around 270 μs to occur as estimated using the Eyring equation[40,41] for the reaction rate

$$k_r = \frac{K_B T}{h} \exp\left[\frac{-AE}{RT}\right]$$

at T = 300 K. Therefore, molecular dynamics simulations will not properly sample this process in computationally accessible times of ps–μs. To efficiently sample molecular events during the DA reaction, we used umbrella sampling[42,43] along the reaction coordinate. The umbrella sampling method adds biasing harmonic potentials to the potential energy landscape

https://doi.org/10.1021/acs.jpcc.1c01901
J. Phys. Chem. C 2021, 125, 14599–14606

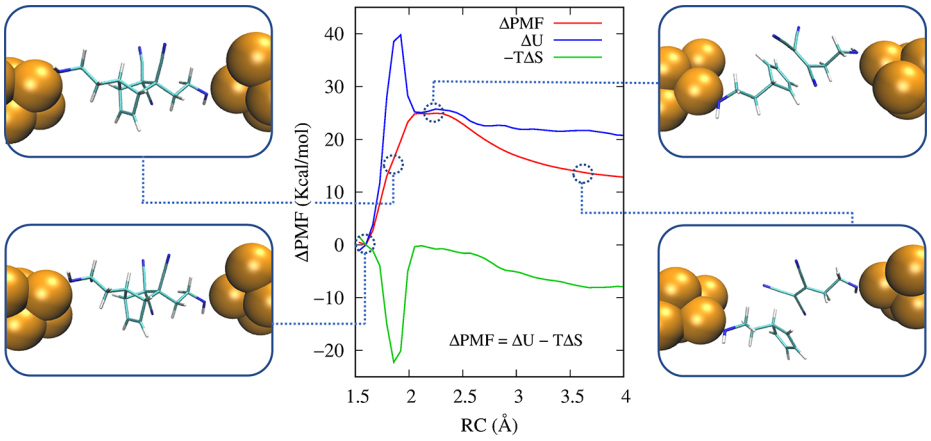

Figure 2. Thermodynamic decomposition of the potential of mean force (PMF) of the Diels–Alder reaction in a junction for the case L = 12.9 Å.

of the process, favoring otherwise rare events in the MD. To recover unbiased thermodynamic properties, we employed the weighted histogram analysis method (WHAM),[44] as implemented in ref 45. As sketched in Figure 1a, the reaction coordinate (RC) was chosen to be the average length of the new bonds formed during the reaction. Collective variables equivalent to this one have been used previously to describe Diels–Alder reactions.[46] The force constants k for the umbrella windows were chosen to be between 50 and 650 kcal mol^{-1} Å^{-2}. The largest values of k were placed around RC = 2–2.5 Å (transition state region), while the lowest values correspond to umbrella windows in the reactants and products regions. This ensures that the high energy regions around the transition state, which are less probable to access during the molecular dynamics, can be properly sampled.

Transport Computations. The application of a bias voltage to a molecular junction leads to charge transport from one electrode to the other, using the molecule in between as the transmission medium. The conductance (G) of the molecular junction during the Diels–Alder reaction was quantified through computation of the transmission coefficient of the system, $T(E)$. In the low bias limit and assuming coherent transport, the transmission coefficient at the Fermi energy of the electrodes is proportional to G,[2] $T(E_F) = G/G_0$, where $G_0 = 2e^2/h$ is the quantum of conductance. To compute the transmission coefficient, we used nonequilibrium Green's functions with an extended Hückel (EH) Hamiltonian, as in ref 47. The EH Hamiltonian captures the essential electronic structure of the system and allows the computation of the conductance of thousands of molecular snapshots from the molecular dynamics simulations, as required to get averages. In our transport computations, the Fermi energy of the electrodes is a simulation parameter chosen to be at −10.92 eV, corresponding to the EH energy of the Au's 6s orbital. This value is expected to be close to the work function of the Au surface in EH, and it is between the HOMO and LUMO of the DA product. Similar values for the EH Fermi energy of gold electrodes were required to match simulations to experimental conductance histograms.[4] Furthermore, while the density of states of the electrodes was considered in the wide band limit approximation, the gold atoms in the dynamics were used to explicitly compute the electrode–molecule couplings.

RESULTS AND DISCUSSION

Figure 1b shows changes in the potential of mean force (ΔPMF) of the DA reaction for values of L ranging from 12.6 to 14.2 Å. The PMF corresponds to the Helmholtz free energy (A) along the reaction coordinate (RC) and succinctly summarizes the thermodynamics of the reaction. For L = 12.9 Å, ΔPMF was computed, choosing the Helmholtz free energy of the product (RC = 1.65 Å) as the zero. To compare the ΔPMF for different values of L, the geometry of the products were optimized using the same level of electronic structure as in the dynamics, and the zero of energy in the PMF profiles was chosen accordingly, keeping the free energy of the product for the case L = 12.9 Å as the zero reference. In all cases, the products region is located around RC = 1.65 Å, there is a wide transition state region in the RC = 2–2.5 Å range, and the reactants region corresponds to RC > 2.5 Å.

In a molecular junction setup, the separation distance between the electrodes can be mechanically manipulated, allowing to tune the degree of reactivity of the system. This is because the activation energy and stability of the products of the DA reaction are highly sensitive to changes in L. Figure 1d shows the activation energy (AE), computed from the PMFs, of the DA reaction for several values of L. For L > 13.7 Å, the AE rapidly increases with increasing L. When the electrodes are brought closer to each other (L < 13.7 Å), the system reaches a region where the activation energy is more favorable for the reaction and approximately independent of L. In the range explored, L ∼ 12.9 Å provides the lowest energy barrier. As a consequence, the characteristic time of the reaction (the inverse of the reaction rate, computed using the Eyring equation) varies over 3 orders of magnitude by varying L just 1.3 Å, from 2.15 × 10^5 μs for the L = 14.2 Å case to 367 μs for L = 12.9 Å! Similarly, Figure 1c shows the relative energy (ΔU^{opt}) of the optimized geometry of the products, which corresponds to the shifted (as in Figure 1b) ΔPMF minimum in the products region. Note that the range of L for which the AE is most favorable (L < 13.7 Å) also corresponds to the range where the products are most stable (lowest ΔU^{opt}), making it optimal for the DA reaction. For even shorter values of L (<12.3 Å), the transition state sampled in the dynamics does not correspond to the DA reaction.

The activation energy barrier of the DA reaction contains contributions from changes in the internal energy and entropy of the system, as it evolves from reactants to the transition state. A natural question to ask is what is the exact contribution

https://doi.org/10.1021/acs.jpcc.1c01901
J. Phys. Chem. C 2021, 125, 14599–14606

from each source? Figure 2 shows the PMF and its thermodynamic decomposition, for the reaction with the lowest activation energy. The contributions to the PMF were obtained by computing binned average potential energies (U) along RC, such that the temperature-modulated entropic contributions ($-TS$) were available through simple subtraction, as detailed in ref 48. As shown, in the activation energy barrier region (~2 < RC < 5 Å) the energy penalty for the reaction is lower (4.10 kcal/mol ≡ 31.9% of the AE) than the entropy penalty (8.75 kcal/mol ≡ 68.1% of the AE). This is expected for reactions with highly ordered transitions states, in which the restrictions in the translation of atoms and rotation of molecular fragments reduce the entropy of the system. Values for the thermodynamic decomposition of the AE for the DA reaction for different values of L are shown in Table 1. In all cases, the entropic contribution to the AE is around 68%, making this reaction entropically limited. In addition, note the sudden increase in the internal energy component at RC ~ 1.8 Å, resulting from the repulsive interactions when the reactants approach each other, is compensated by a gain in entropy once the system transitions to the products and leaves the highly ordered transition state. This was corroborated with the molecular dynamics simulations for which key snapshots can be seen in Figure 2. To demonstrate that these results do not depend strongly on the choice of anchor group, we repeated the computations for L = 12.9 Å using thiol anchor groups. The results in Figure S1 (Supporting Information) demonstrate that the PMF and its thermodynamic decomposition remain essentially unaltered.

Table 1. Thermodynamic Decomposition of the Activation Energy, AE, for the DA Reaction in Junctions with Different Separation Distance between Electrodes, L (Å)[a]

L	AE	ΔU	$-T\Delta S$
12.3	13.00	4.38	8.62 (66.3%)
12.6	12.96	3.97	8.99 (69.4%)
12.9	12.85	4.10	8.75 (68.1%)
13.2	13.37	4.33	9.04 (67.6%)
13.5	13.23	3.76	9.47 (71.6%)
13.8	14.23	4.12	10.11 (71.0%)
14.2	16.66	5.85	10.81 (64.9%)

[a]The values in parentheses are the percentage of the entropic contribution to the AE. All energies are reported in kcal/mol.

The results above show that the activation energy of the DA reaction in the junction setup is mostly entropic in origin. Therefore, any strategy directed to decrease the entropy gap between the reactants and the transition state (for instance, by using rigid anchor groups) or reduce the entropic contribution to the PMF (lowering the temperature), is expected to reduce this thermodynamic barrier.

How is this reaction affected by changes in the temperature of the system? Figure 3 shows the PMF, its thermodynamic decomposition, and the activation energy of the DA reaction in the junction setup at different temperatures. As shown in Figure 3a, lower temperatures result in PMF whose associated activation energy is smaller. Table 2 shows the contributions from the internal energy and entropy to the activation energy of the DA reaction for these temperatures. The changes in the internal energy (ΔU) of the system are mildly dependent on the temperature, going from 3.01 kcal/mol for T = 100 K to 4.10 kcal/mol for T = 300 K. By contrast, the changes in entropy are modulated by T and as shown in Figure 3b for three selected cases, this leads to a clear change in the $-T\Delta S$ contribution to the PMF, especially in the reactants region (RC > 2.5 Å). As a result, the entropic contribution to the activation energy is lower for colder systems. Note that the decrease of the activation energy when lowering the temperature does not necessarily imply the increase of the reaction

Table 2. Thermodynamic Decomposition of the Activation Energy, AE, for the DA Reaction in the Junction with L = 12.9 Å, at Different Temperatures, T (K)[a]

T	AE	ΔU	$-T\Delta S$
100	7.28	3.01	4.27 (58.6%)
150	8.37	3.38	4.99 (59.6%)
200	9.89	3.49	6.40 (64.7%)
250	11.37	3.84	7.53 (66.2%)
300	12.85	4.10	8.75 (68.1%)

[a]The values in parentheses are the percentage contribution of the entropy to the AE. All energies are reported in kcal/mol.

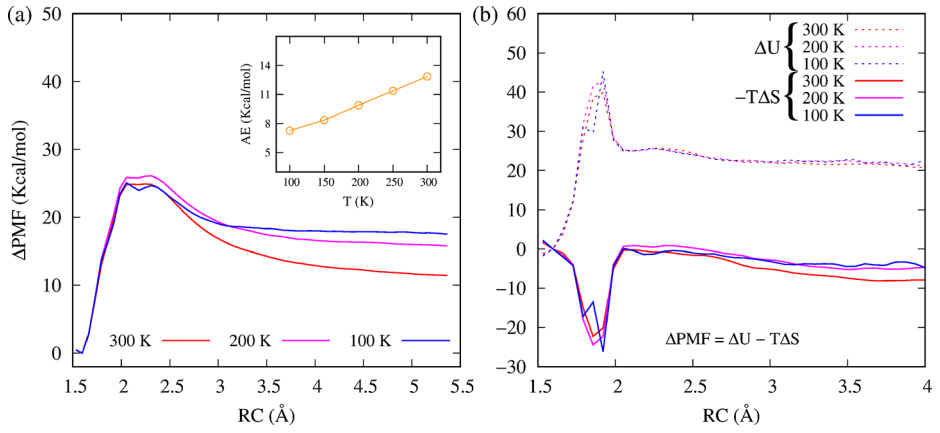

Figure 3. Potential of mean force (PMF) and thermodynamic decomposition of the Diels–Alder (DA) reaction in a junction at different temperatures. (a) PMF of the DA reaction to form a molecular junction at three representative temperatures, considering L = 12.9 Å. The inset shows the activation energy as a function of the temperature. (b) Thermodynamic decomposition of the PMF for three representative temperatures. Note that the activation energy decreases when lowering the temperature due to the decrease of the entropic contribution.

https://doi.org/10.1021/acs.jpcc.1c01901
J. Phys. Chem. C 2021, 125, 14599−14606

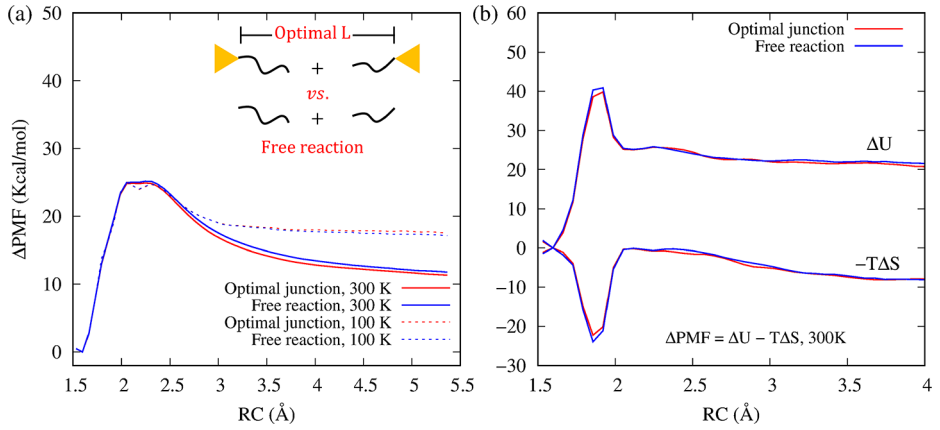

Figure 4. Potential of mean force (PMF) and thermodynamic decomposition of the Diels–Alder (DA) reaction in an optimal junction (L = 12.9 Å) and without electrodes (free reaction). (a) PMF of the DA reaction at 100 and 300 K. (b) Thermodynamic decomposition of the PMF at 300 K. Note that the optimal junction exhibits the same features as the free reaction.

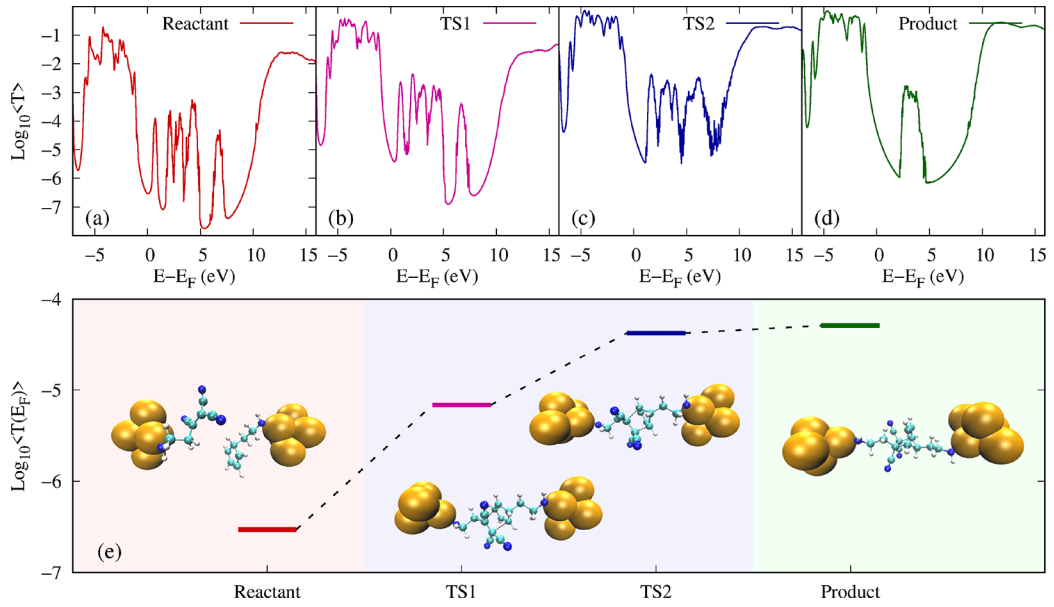

Figure 5. Average transmission spectra and relevant transmission changes in representative stages of the Diels–Alder (DA) reaction in a molecular junction. (a–d) Average transmission spectra for 8000 molecular structures in the region of products, transition state (TS1 and TS2) and reactants of the DA reaction, respectively. (e) Average transmission coefficient at the Fermi energy of the electrodes for the relevant stages of the DA reaction. Note that the formation of a molecular junction due to the DA reaction is signaled with an increase in the transmission coefficient.

rate. This is because lowering the temperature also reduces the thermal energy of the system. However, low activation energy barriers can be overcome by nonthermal sources such as the mechanical manipulation of the junction.

How different is a DA reaction taking place in a junction setup with respect to the equivalent free reaction where the reactants are not attached to electrodes? To address this, we performed MD simulations of the reaction in the absence of electrodes and added hydrogens to the terminal atoms. In this case, the only restriction to the dynamics was that of the umbrella sampling to the RC. In our simulations, the lowest activation energy for the DA reaction in the junction setup (12.85 kcal/mol, for L = 12.9 Å) essentially coincides with that of the free reaction (12.66 kcal/mol). In fact, as shown in Figure 4, the PMF of the optimal junction (a junction with a value of L in the region where the activation energy is the lowest; for definitiveness, we use L = 12.9 Å) exhibits the same features as the free reaction. Any variation of L that takes the junction out of the optimal region imposes a constraint to the process. This is contrary to what is observed in metal-catalyzed reactions[49−51] or confinement-enhanced processes,[52−54] where the confinement and/or the presence of the metallic surfaces help driving forward the process.

In addition to spatial constraints, the electrodes can introduce changes in the electronic structure of the reactants. Here those effects were minimized by the short alkyl chains that uncouple the reactive center from the electrodes. This is in contrast to previous experiments in which the reactants have been directly anchored to the electrodes.[27]

The junction setup where the reaction takes place not only allows us to apply mechanical forces and bring the reactants together in a controllable fashion but also makes it possible to apply bias voltages on the system and measure the resulting current to monitor the process. It has been shown previously that the changes in the electronic structure of a molecular junction due to changes in the molecular geometry can be

https://doi.org/10.1021/acs.jpcc.1c01901
J. Phys. Chem. C 2021, 125, 14599−14606

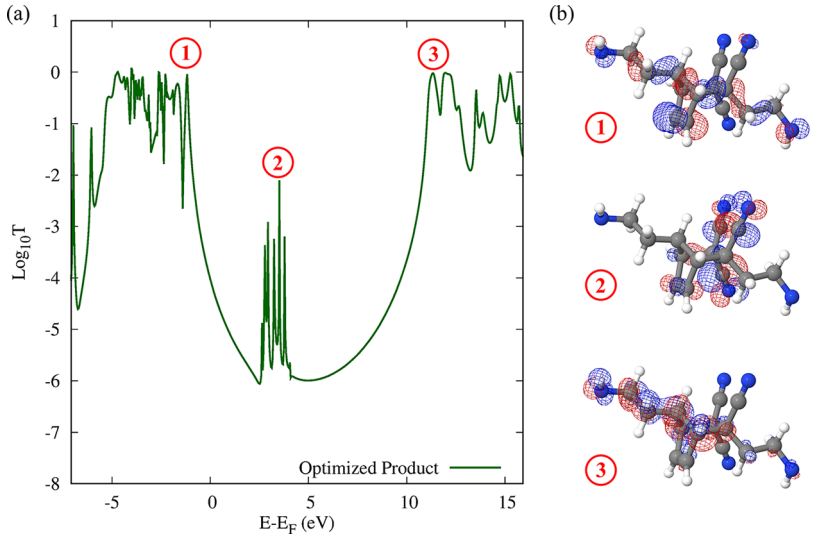

Figure 6. (a) Transmission spectrum of the optimized product **3**. (b) Molecular orbitals associated with the highlighted transmission peaks. 1 is the HOMO and 2 and 3 are LUMO+*n* orbitals.

monitored by measuring the conductance.[1,13] When the DA reaction takes place in a junction, through-bond conduction channels between the electrodes are created, and therefore, an increase in the conductance is expected. In our molecular dynamics simulations, the gold atoms are used to represent the explicit part of the electrodes that is connected to the molecular region.

Figure 5 shows the average transmission spectra, and the corresponding average conductance, of the junction at different stages of the DA reaction. Each average in this figure was computed from 8000 molecular structures encountered in the dynamics. Because the observed transition state region is relatively wide in the RC coordinate, we chose two separated points to represent it, TS1 and TS2, corresponding to RC = 2.5 and 2.0 Å, respectively. The reactants and products region corresponds to structures whose RC = 1.5 and 5.4 Å, respectively. The average transmission coefficient at the Fermi energy of the electrodes (E_F), which is proportional to the conductance in the low bias limit, is shown in Figure 5e. As can be seen, the conductance of the system increases ∼2.5 orders of magnitude when the reaction occurs. To demonstrate that these results are independent of the anchor group, we repeated the computations with thiol linkers (see Figure S2, Supporting Information), obtaining similar results. Thus, in experiments, successful reactions are expected to result in sudden increases of the conductance.

To understand the contributions of individual molecular orbitals to the average transmission spectra (Figure 5), Figure 6 shows the transmission spectrum of the product **3** at L = 12.9 Å and the molecular orbitals associated with highlighted peaks 1−3. The highly transmissive peak 1 due to the HOMO dominates the transmission of the junction at E_F. The LUMO +*n* low transmission peaks 2 are associated with highly localized orbitals on the CN groups that do not couple effectively to the electrodes. The peak at 3 that exhibits high transmission is due to an unoccupied molecular orbital with significant coupling to the electrodes.

CONCLUSIONS

Our simulations show that the degree of reactivity of the DA reaction can be mechanically controlled in a junction setup. The mechanical control of the reactivity arises because the activation energy and stability of the products of the DA reaction in the Au−molecule−Au junction are highly sensitive to changes in the separation distance between the electrodes, L. This is a parameter that can be controlled in experiments in which a tip is mechanically brought closer to a surface, as in AFM or STM-like experiments.

Furthermore, by computing the internal energy and entropic contributions to the PMF, we found that the activation energy of the DA reaction is mostly entropic. This prevents this kind of association reaction to occur efficiently at the single-entity limit. However, our results show that the activation energy decreases at low temperatures, opening the possibility of using nonthermal sources such as mechanical manipulation to trigger the reactive effect. Nevertheless, high temperatures still result in higher reaction rates for the thermally activated process.

Surprisingly, when the separation distance between the electrodes is optimal, the thermodynamics of the DA reaction in the junction setup essentially coincides with the thermodynamics of the free reaction. This implies that under appropriate conditions, the observations made in a controllable junction setup can be extrapolated to the reaction in the absence of electrodes and vice versa.

Importantly, through charge transport computations of the thermally accessible structures along the reaction, we exemplified how the junction setup can be used to monitor the occurrence of the reaction by measuring the conductance of the system. Specifically, because successful reactions lead to the formation of molecular junctions, these events can be identified as sudden increases in the current, allowing on-the-fly monitoring of the process.

Last, although in regular DA reactions the system can reach different transition states that lead to different conformations, in all our simulations the obtained product always corresponds to the same stereoisomer. This is because by attaching the reactants to the electrodes from specific positions, the transition state is forced to adopt a specific configuration. This suggests that the junction setup can potentially lead to mechanical control of the stereoselectivity of the DA reaction.

https://doi.org/10.1021/acs.jpcc.1c01901
J. Phys. Chem. C 2021, 125, 14599−14606

■ ASSOCIATED CONTENT

Supporting Information

The Supporting Information is available free of charge at https://pubs.acs.org/doi/10.1021/acs.jpcc.1c01901.

Potential of mean force and transport computations of the DA reaction with thiol anchor groups (PDF)

■ AUTHOR INFORMATION

Corresponding Author

Ignacio Franco − *Department of Chemistry, University of Rochester, Rochester, New York 14627−0216, United States; Department of Physics, University of Rochester, Rochester, New York 14611−0216, United States;* orcid.org/0000-0002-0802-8185; Email: ignacio.franco@rochester.edu

Authors

Leopoldo Mejía − *Department of Chemistry, University of Rochester, Rochester, New York 14627−0216, United States;* orcid.org/0000-0003-4534-0191

Diego Garay-Ruiz − *Institute of Chemical Research of Catalonia (ICIQ), The Barcelona Institute of Science and Technology (BIST), 43007 Tarragona, Spain;* orcid.org/0000-0003-0744-0562

Complete contact information is available at: https://pubs.acs.org/10.1021/acs.jpcc.1c01901

Author Contributions

[§]These authors contributed equally to this work.

Author Contributions

D.G. performed all electronic structure computations, MD simulations, and thermodynamic decompositions and designed the chemical motifs. L.M. performed the transport computations. I.F. and L.M. designed the project and wrote the paper with contributions from all authors. I.F. overviewed the project.

Notes

The authors declare no competing financial interest.

■ ACKNOWLEDGMENTS

The authors thank the National Science Foundation under grant no. CHE-1553939 and the i-Scholar program of the University of Rochester for support.

■ REFERENCES

(1) Mejía, L.; Renaud, N.; Franco, I. Signatures of Conformational Dynamics and Electrode-Molecule Interactions in the Conductance Profile During Pulling of Single-Molecule Junctions. *J. Phys. Chem. Lett.* **2018**, *9*, 745−750.

(2) Elke, S.; Carlos, C. J. *Molecular Electronics: An Introduction to Theory and Experiment*; World Scientific, 2017; Vol. *15*.

(3) Datta, S. *Quantum transport: Atom to transistor*; Cambridge University Press, 2005.

(4) Li, Z.; Mejía, L.; Marrs, J.; Jeong, H.; Hihath, J.; Franco, I. Understanding the Conductance Dispersion of Single-Molecule Junctions. *J. Phys. Chem. C* **2021**, *125*, 3406−3414.

(5) Segal, D.; Agarwalla, B. K. Vibrational Heat Transport in Molecular Junctions. *Annu. Rev. Phys. Chem.* **2016**, *67*, 185−209.

(6) Li, Q.; Duchemin, I.; Xiong, S.; Solomon, G. C.; Donadio, D. Mechanical Tuning of Thermal Transport in a Molecular Junction. *J. Phys. Chem. C* **2015**, *119*, 24636−24642.

(7) Carpio-Martínez, P.; Hanna, G. Nonequilibrium Heat Transport in a Molecular Junction: A Mixed Quantum-Classical Approach. *J. Chem. Phys.* **2019**, *151*, 074112.

(8) Kim, W. Y.; Choi, Y. C.; Min, S. K.; Cho, Y.; Kim, K. S. Application of Quantum Chemistry to Nanotechnology: Electron and Spin Transport in Molecular Devices. *Chem. Soc. Rev.* **2009**, *38*, 2319−2333.

(9) Deng, X.; Zhang, Z.; Tang, G.; Fan, Z.; Sun, L.; Li, C. Modulation of the Spin Transport Properties of the Iron-Phthalocyanine Molecular Junction by Carbon Chains with Different Connection Sites. *Org. Electron.* **2016**, *35*, 1−5.

(10) Ballmann, S.; Härtle, R.; Coto, P. B.; Elbing, M.; Mayor, M.; Bryce, M. R.; Thoss, M.; Weber, H. B. Experimental Evidence for Quantum Interference and Vibrationally Induced Decoherence in Single-Molecule Junctions. *Phys. Rev. Lett.* **2012**, *109*, 056801.

(11) Guédon, C. M.; Valkenier, H.; Markussen, T.; Thygesen, K. S.; Hummelen, J. C.; Van Der Molen, S. J. Observation of Quantum Interference in Molecular Charge Transport. *Nat. Nanotechnol.* **2012**, *7*, 305−309.

(12) Garner, M. H.; Li, H.; Chen, Y.; Su, T. A.; Shangguan, Z.; Paley, D. W.; Liu, T.; Ng, F.; Li, H.; Xiao, S.; et al. Comprehensive Suppression of Single-Molecule Conductance Using Destructive σ-Interference. *Nature* **2018**, *558*, 415−419.

(13) Mejía, L.; Franco, I. Force-Conductance Spectroscopy of a Single-Molecule Reaction. *Chem. Sci.* **2019**, *10*, 3249−3256.

(14) Koch, M.; Li, Z.; Nacci, C.; Kumagai, T.; Franco, I.; Grill, L. How Structural Defects Affect the Mechanical and Electrical Properties of Single Molecular Wires. *Phys. Rev. Lett.* **2018**, *121*, 047701.

(15) Pirrotta, A.; De Vico, L.; Solomon, G. C.; Franco, I. Single-Molecule Force-Conductance Spectroscopy of Hydrogen-Bonded Complexes. *J. Chem. Phys.* **2017**, *146*, 092329.

(16) Wu, C.; Bates, D.; Sangtarash, S.; Ferri, N.; Thomas, A.; Higgins, S. J.; Robertson, C. M.; Nichols, R. J.; Sadeghi, H.; Vezzoli, A. Folding a Single-Molecule Junction. *Nano Lett.* **2020**, *20*, 7980−7986.

(17) Franco, I.; George, C. B.; Solomon, G. C.; Schatz, G. C.; Ratner, M. A. Mechanically Activated Molecular Switch through Single-Molecule Pulling. *J. Am. Chem. Soc.* **2011**, *133*, 2242−2249.

(18) Li, L.; Lo, W.-Y.; Cai, Z.; Zhang, N.; Yu, L. Proton-Triggered Switch Based on a Molecular Transistor with Edge-On Gate. *Chem. Sci.* **2016**, *7*, 3137−3141.

(19) Lang, N. D.; Solomon, P. M. Charge Control in a Model Biphenyl Molecular Transistor. *Nano Lett.* **2005**, *5*, 921−924.

(20) Ghosh, A. W.; Rakshit, T.; Datta, S. Gating of a Molecular Transistor: Electrostatic and Conformational. *Nano Lett.* **2004**, *4*, 565−568.

(21) Fathizadeh, S.; Behnia, S.; Ziaei, J. Engineering DNA Molecule Bridge between Metal Electrodes for High-Performance Molecular Transistor: An Environmental Dependent Approach. *J. Phys. Chem. B* **2018**, *122*, 2487−2494.

(22) Díez-Pérez, I.; Hihath, J.; Lee, Y.; Yu, L.; Adamska, L.; Kozhushner, M. A.; Oleynik, I. I.; Tao, N. Rectification and Stability of a Single Molecular Diode with Controlled Orientation. *Nat. Chem.* **2009**, *1*, 635−641.

(23) Elbing, M.; Ochs, R.; Koentopp, M.; Fischer, M.; von Hänisch, C.; Weigend, F.; Evers, F.; Weber, H. B.; Mayor, M. A Single-Molecule Diode. *Proc. Natl. Acad. Sci. U. S. A.* **2005**, *102*, 8815−8820.

(24) Jia, C.; Migliore, A.; Xin, N.; Huang, S.; Wang, J.; Yang, Q.; Wang, S.; Chen, H.; Wang, D.; Feng, B.; et al. Covalently Bonded Single-Molecule Junctions with Stable and Reversible Photoswitched Conductivity. *Science* **2016**, *352*, 1443−1445.

(25) Guan, J.; Jia, C.; Li, Y.; Liu, Z.; Wang, J.; Yang, Z.; Gu, C.; Su, D.; Houk, K. N.; Zhang, D.; et al. Direct Single-Molecule Dynamic Detection of Chemical Reactions. *Sci. Adv.* **2018**, *4*, eaar2177.

(26) Li, Y.; Haworth, N. L.; Xiang, L.; Ciampi, S.; Coote, M. L.; Tao, N. Mechanical Stretching-Induced Electron-Transfer Reactions and Conductance Switching in Single Molecules. *J. Am. Chem. Soc.* **2017**, *139*, 14699−14706.

(27) Aragones, A. C.; Haworth, N. L.; Darwish, N.; Ciampi, S.; Bloomfield, N. J.; Wallace, G. G.; Diez-Perez, I.; Coote, M. L.

Electrostatic Catalysis of a Diels-Alder Reaction. *Nature* **2016**, *531*, 88−91.
(28) Huang, C.; Jevric, M.; Borges, A.; Olsen, S. T.; Hamill, J. M.; Zheng, J.-T.; Yang, Y.; Rudnev, A.; Baghernejad, M.; Broekmann, P.; et al. Single-Molecule Detection of Dihydroazulene Photo-Thermal Reaction using Break Junction Technique. *Nat. Commun.* **2017**, *8*, 15436.
(29) Oh, T.; Rally, M. Reagent-Controlled Asymmetric Diels-Alder Reactions. A Review. *Org. Prep. Proced. Int.* **1994**, *26*, 129−158.
(30) Martin, J. G.; Hill, R. K. Stereochemistry of the Diels-Alder Reaction. *Chem. Rev.* **1961**, *61*, 537−562.
(31) Kwart, H.; King, K. The Reverse Diels-Alder or Retrodiene Reaction. *Chem. Rev.* **1968**, *68*, 415−447.
(32) Hernandez Mancera, J. P.; Núñez-Zarur, F.; Gutiérrez-Oliva, S.; Toro-Labbé, A.; Vivas-Reyes, R. Diels-Alder Reaction Mechanisms of Substituted Chiral Anthracene: A Theoretical Study Based on the Reaction Force and Reaction Electronic Flux. *J. Comput. Chem.* **2020**, *41*, 2022−2032.
(33) Rojas-Valencia, N.; Núñez-Zarur, F. The Origin of the High Reactivity of Triazolinediones (TADs) in Diels-Alder Reactions from a Theoretical Perspective. *Tetrahedron* **2020**, *76*, 131459.
(34) Van Duin, A. C.; Dasgupta, S.; Lorant, F.; Goddard, W. A. ReaxFF: a Reactive Force field for Hydrocarbons. *J. Phys. Chem. A* **2001**, *105*, 9396−9409.
(35) Senftle, T. P.; Hong, S.; Islam, M. M.; Kylasa, S. B.; Zheng, Y.; Shin, Y. K.; Junkermeier, C.; Engel-Herbert, R.; Janik, M. J.; Aktulga, H. M.; et al. The ReaxFF Reactive Force-Field: Development, Applications and Future Directions. *NPJ. Comput. Mater.* **2016**, *2*, 1−14.
(36) Larsen, A. H.; Mortensen, J. J.; Blomqvist, J.; Castelli, I. E.; Christensen, R.; Du lak, M.; Friis, J.; Groves, M. N.; Hammer, B.; Hargus, C.; et al. The Atomic Simulation Environment-a Python Library for Working with Atoms. *J. Phys.: Condens. Matter* **2017**, *29*, 273002.
(37) Aradi, B.; Hourahine, B.; Frauenheim, T. DFTB+, a Sparse Matrix-Based Implementation of the DFTB Method. *J. Phys. Chem. A* **2007**, *111*, 5678−5684.
(38) Fihey, A.; Hettich, C.; Touzeau, J.; Maurel, F.; Perrier, A.; Köhler, C.; Aradi, B.; Frauenheim, T. SCC-DFTB Parameters for Simulating Hybrid Gold-Thiolates Compounds. *J. Comput. Chem.* **2015**, *36*, 2075−2087.
(39) Zang, Y.; Pinkard, A.; Liu, Z.-F.; Neaton, J. B.; Steigerwald, M. L.; Roy, X.; Venkataraman, L. Electronically Transparent Au-N Bonds for Molecular Junctions. *J. Am. Chem. Soc.* **2017**, *139*, 14845−14848.
(40) Eyring, H. The Activated Complex in Chemical Reactions. *J. Chem. Phys.* **1935**, *3*, 107−115.
(41) Eyring, H. The Activated Complex and the Absolute Rate of Chemical Reactions. *Chem. Rev.* **1935**, *17*, 65−77.
(42) Torrie, G. M.; Valleau, J. P. Nonphysical Sampling Distributions in Monte Carlo Free-Energy Estimation: Umbrella Sampling. *J. Comput. Phys.* **1977**, *23*, 187−199.
(43) Kästner, J. Umbrella Sampling. *Wiley Interdiscip. Rev. Comput. Mol. Sci.* **2011**, *1*, 932−942.
(44) Kumar, S.; Rosenberg, J. M.; Bouzida, D.; Swendsen, R. H.; Kollman, P. A. The Weighted Histogram Analysis Method for Free-Energy Calculations on Biomolecules. I. The Method. *J. Comput. Chem.* **1992**, *13*, 1011−1021.
(45) Grossfield, A. *WHAM: the Weighted Histogram Analysis Method, Version 2.0.9*. Available at membrane.urmc.rochester.edu/content/wham.
(46) Zhang, X.; Bruice, T. C. Diels- Alder Ribozyme Catalysis: A Computational Approach. *J. Am. Chem. Soc.* **2007**, *129*, 1001−1007.
(47) Hutcheson, J.; Franco, I.; Renaud, N.; Carignano, M.; Ratner, M. A.; Schatz, G. C. TRANSpull: Computes Pulling Coupled to Transport Properties of Single Molecules. 2011; https://nanohub.org/resources/11739.
(48) Franco, I.; Schatz, G. C.; Ratner, M. A. Single-Molecule Pulling and the Folding of Donor-Acceptor Oligorotaxanes: Phenomenology and Interpretation. *J. Chem. Phys.* **2009**, *131*, 124902.
(49) Sanchez, A.; Abbet, S.; Heiz, U.; Schneider, W.-D.; Häkkinen, H.; Barnett, R.; Landman, U. When Gold is not Noble: Nanoscale Gold Catalysts. *J. Phys. Chem. A* **1999**, *103*, 9573−9578.
(50) Barluenga, J.; Fernández-Rodríguez, M. Á.; García-García, P.; Aguilar, E. Gold-Catalyzed Intermolecular Hetero-Dehydro-Diels-Alder Cycloaddition of Captodative Dienynes with Nitriles: a New Reaction and Regioselective Direct Access to Pyridines. *J. Am. Chem. Soc.* **2008**, *130*, 2764−2765.
(51) Mejía, L.; Ferraro, F.; Osorio, E.; Hadad, C. Z. Activation and Diffusion of Ammonia Borane Hydrogen on Gold Tetramers. *Int. J. Quantum Chem.* **2018**, *118*, e25567.
(52) Pirrotta, A.; Solomon, G. C.; Franco, I. Hydrogen Bonding in Tight Environments: Simulated Force Spectroscopy of Nanoconfined Hydrogen-Bonded Complexes. *J. Phys. Chem. C* **2016**, *120*, 19470−19478.
(53) Yu, C.; He, J. Synergic Catalytic Effects in Confined Spaces. *Chem. Commun.* **2012**, *48*, 4933−4940.
(54) Mejía, L.; Hadad, C. Effect of the Euclidean Dimensionality on the Energy Transfer Up-Conversion Luminescence. *J. Photochem. Photobiol., A* **2019**, *382*, 111908.

https://doi.org/10.1021/acs.jpcc.1c01901
J. Phys. Chem. C 2021, 125, 14599−14606